PHYSICAL REVIEW D **87,** 083008 (2013)

How massless neutrinos affect the cosmic microwave background damping tail

Zhen Hou,[1] Ryan Keisler,[2] Lloyd Knox,[1] Marius Millea,[1] and Christian Reichardt[3]
[1]*Department of Physics, One Shields Avenue, University of California, Davis, California 95616, USA*
[2]*Department of Astronomy and Astrophysics, University of Chicago, 5640 S. Ellis Avenue, Chicago, Illinois 60637, USA*
[3]*Department of Physics, University of California, Berkeley, California 94720, USA*
(Received 12 April 2011; revised manuscript received 20 August 2012; published 23 April 2013)

We explore the physical origin and robustness of constraints on the energy density in relativistic species prior to and during recombination, often expressed as constraints on an effective number of neutrino species, $N_{\rm eff}$. If the primordial helium abundance, $Y_{\rm P}$, follows the prediction of the big bang nucleosynthesis (BBN) theory, the constraint on $N_{\rm eff}$ from current cosmic microwave background anisotropy data is almost entirely due to the impact of the neutrinos on the expansion rate, and how those changes to the expansion rate alter the ratio of the photon diffusion scale to the sound horizon scale at recombination. We demonstrate that, as long as the primordial helium abundance is derived in a BBN-consistent manner, the constraint on $N_{\rm eff}$ degrades little after marginalizing over $A_{\rm eISW}$, the phenomenological parameter characterizing the amplitude of the early Integrated Sachs-Wolfe (ISW) effect. We also provide a first determination of $A_{\rm eISW}$. Varying the $Y_{\rm P}$ also changes the ratio of damping to sound horizon scales. We study the physical effects that prevent the resulting near degeneracy between $N_{\rm eff}$ and $Y_{\rm P}$ from being a complete one and find that the early ISW effect does play a role in breaking this degeneracy. Examining light-element abundance measurements, we see no significant evidence for the evolution of $N_{\rm eff}$ and the baryon-to-photon ratio from the epoch of BBN to decoupling. Finally, we consider measurements of the distance-redshift relation at low to intermediate redshifts and their implications for the value of $N_{\rm eff}$.

DOI: 10.1103/PhysRevD.87.083008 PACS numbers: 98.70.Vc, 14.60.St

I. INTRODUCTION

High-resolution observations of the cosmic microwave background (CMB) temperature anisotropy are providing a precise measurement of the damping tail of CMB power spectrum, shedding light on the physical conditions during recombination and back into the radiation-dominated era. The measurements have revealed somewhat less fluctuation power at small angular scales than expected in the standard cosmological model [1–4]. Many papers [3–9] have considered the possibility that this deficit of power is due to extra (dark) relativistic species [10], such as nearly massless sterile neutrinos. Constraints are usually expressed in terms of an effective number of neutrinos, $N_{\rm eff}$ [11].

Note that these constraints apply to any weakly interacting or noninteracting species that is relativistic at recombination. Hypothesized additional species include sterile neutrinos; sub-eV-mass axions as in, e.g., Ref. [12]; and those arising in many other extensions of the standard model, such as in Ref. [13].

Interest in the number of light degrees of freedom is further stimulated by i) recent inferences of the primordial helium abundance which are larger, and with larger uncertainties than previous analyses [14–16], ii) evidence for additional (sterile) neutrino species from laboratory-produced neutrinos [17] and reactor-produced neutrinos [18], and iii) a slight tension between determinations of distance vs redshift at very low redshifts (essentially measurements of H_0 [19]) and those at low to intermediate redshifts that use the baryon acoustic oscillation (BAO) feature in the galaxy power spectrum as a CMB-calibrated standard ruler [20,21].

Given this interest, and impending improvements to the damping tail measurements from the SPT [4] (K11 hereafter) and the Planck satellite, a pedagogical exposition of the impact of $N_{\rm eff}$ on the CMB is quite timely. The relevant physics is beautifully simple and deserves to be as well (and as broadly) understood as the constraints on $N_{\rm eff}$ from BBN considerations. Focusing on the physics behind the constraints also allows one to understand their more general implications. The only important assumptions about the relativistic degrees of freedom that go into the CMB predictions are that their interactions are negligible and they are massless.

Despite the analyses provided by Refs. [22,23], we find that the mechanism for constraining $N_{\rm eff}$ is not broadly understood, and is in some cases misunderstood. The sensitivity to $N_{\rm eff}$ from high-resolution CMB observations is due to the impact of the mean relativistic energy density on the Universe's expansion rate prior to (and during) the epoch of photon-baryon decoupling. As we demonstrate below, neutrino perturbations do not play a significant role [24], nor do anisotropies induced after decoupling. To study how much the early ISW effect plays a role in the estimation of $N_{\rm eff}$, we introduce a phenomenological scaling of its physical value by a parameter $A_{\rm eISW}$ and examine the constraints on $N_{\rm eff}$ that follow from marginalizing over $A_{\rm eISW}$.

The constraints on $N_{\rm eff}$ are model dependent; there are other ways to extend the standard cosmological model

to suppress small-scale power in the cosmic microwave background. We discuss, in particular, departing from a power law for the primordial perturbation spectrum, and allowing the fraction of baryonic mass in helium, Y_P, to be a free parameter.

We also consider the sensitivity of inferences of $N_{\rm eff}$ from CMB data to assumptions about BBN and measurements of light-element abundances. Allowing Y_P to vary freely introduces a degeneracy that completely changes the mechanism by which $N_{\rm eff}$ is constrained by CMB data. We comment on the origin of constraints in the $N_{\rm eff}$-Y_P plane.

In Sec. II, we review the analytic explanation for the origin of constraints on $N_{\rm eff}$ from CMB observations and demonstrate its quantitative effectiveness in understanding constraints from current data. We also examine the model dependence of constraints on $N_{\rm eff}$. In Sec. III, we consider the impact of the early ISW effect on $N_{\rm eff}$ constraints, and we discuss our results and conclude in Sec. IV.

II. HOW CMB OBSERVATIONS CONSTRAIN COMPONENT DENSITIES

Let us review the sensitivity of the CMB power spectrum to the densities today of baryons, ρ_b, cold dark matter plus baryons, ρ_m, and dark energy, ρ_Λ, all within the context of the ΛCDM model [25]. For more details than we give here, see Refs. [26,27]. In the course of our review, we will identify directions in parameter space that cause large changes in probability density. When we do study variations in $N_{\rm eff}$, we will do so along orthogonal directions.

A. Sensitivity to the non-neutrino components

The dependence of the CMB on ρ_b arises from the dependence of the equation of state of the pre-recombination plasma on the fraction of its energy density that comes from baryons. Increasing the number of baryons per photon decreases the plasma's pressure-to-density ratio (P/ρ). The resulting shift in the equilibrium point between gravitational and pressure forces alters the ratio of even-peak heights to odd-peak heights. We know the energy density of photons very well from measuring the CMB photon spectrum [28], and can thus infer ρ_b from the ratio of even to odd peak heights.

The dependence on ρ_m arises from the sensitivity of the evolution of a Fourier mode amplitude to the fraction of the energy density contributed by nonrelativistic matter when the mode's wavelength is equal to the Hubble radius. This ratio depends on $\lambda/r_{\rm EQ}$, where λ is the comoving wavelength, $r_{\rm EQ} = H_{\rm EQ}^{-1}/a_{\rm EQ}$ defines the comoving Hubble radius at the time when the matter density equals the radiation density (an epoch denoted by "EQ"), and a is the scale factor parameterizing the expansion of the Universe. The amplitude of a mode projecting to angular scale θ depends on $\theta/\theta_{\rm EQ}$, where $\theta_{\rm EQ} = r_{\rm EQ}/D_A$ because $\theta/\theta_{\rm EQ} = \lambda/r_{\rm EQ}$. Since the amplitude is a strong function of this ratio, there is strong sensitivity to $\theta_{\rm EQ}$, and therefore to $z_{\rm EQ}$ ($1 + z = 1/a$), since assuming the dark energy is a cosmological constant, $\theta_{\rm EQ} = I(\Omega_m)/\sqrt{1 + z_{\rm EQ}}$, where $I(\Omega_m)$ is a very slowly varying function of Ω_m [29].

Thus, the CMB power spectrum is sensitive to $1 + z_{\rm EQ} = \rho_m/\rho_r$. If we *assume* the standard radiation content ($N_{\rm eff} = 3.046$, $\rho_r = \rho_\gamma + \rho_\nu$), then a constraint on $1 + z_{\rm EQ}$ directly constrains ρ_m. However, if we are allowing $N_{\rm eff}$ to vary, we should study its effects at fixed $1 + z_{\rm EQ}$, since this quantity is well constrained by the data. Prior to the CMB damping scale measurements, there were already hints of high $N_{\rm eff}$ by combining the $1 + z_{\rm EQ}$ constraint from WMAP with late-time observables sensitive to the matter density [30].

We now consider ρ_Λ. The angular scales of the acoustic peaks are highly sensitive to the angular size of the sound horizon, $\theta_s = r_s/D_A$. Thus, θ_s is very precisely determined by the data. Given r_s, we could infer D_A. In a universe with zero mean spatial curvature, $D_A = \int cdt/a$ from the time of last scattering to today, and depends only on ρ_m and ρ_Λ. We do know r_s, to some degree, from our determination of ρ_b and ρ_m as described above. These densities determine the history of the sound speed, c_s [31] and the expansion rate, allowing us to calculate r_s, since it depends on no other parameters in the six-parameter ΛCDM model. This determination of r_s allows for a constraint on ρ_Λ.

B. The effect of relativistic and dark degrees of freedom

Changing $N_{\rm eff}$ only slightly alters the above story about the origins of the parameter constraints. We expect inferences of ρ_b, $1 + z_{\rm EQ}$ and θ_s to be nearly unaffected. In the top panel of Fig. 1, we thus hold these parameters fixed while varying $N_{\rm eff}$ from 2 to 6. We hold $z_{\rm EQ}$ fixed by increasing the density of cold dark matter as we increase $N_{\rm eff}$. We keep θ_s fixed by changing ρ_Λ to adjust D_A.

As can be seen in Fig. 1, increasing $N_{\rm eff}$ along the chosen direction in parameter space makes very little difference at low ℓ (exactly as intended) and an increasing difference at higher ℓ. A similar exercise was performed in Ref. [32], in which the authors identified the same parameters to be held fixed. They were interested in the region of the first three peaks and ascribed the relative drop in power toward the third peak to a post-decoupling effect known as the "early integrated Sachs-Wolfe effect." We claim, in contrast, that the drop in power in the damping tail (beyond the second and third peaks) is almost entirely due to increased Silk damping, caused by the increased expansion rate. To demonstrate that the variation is not predominantly due to ISW, in the central panel we have normalized the spectra at $\ell = 400$, where the ISW effect is negligible; we see that the high-ℓ variation is only slightly reduced.

Temperature anisotropies on scales smaller than the photon diffusion length are damped by the diffusion, a

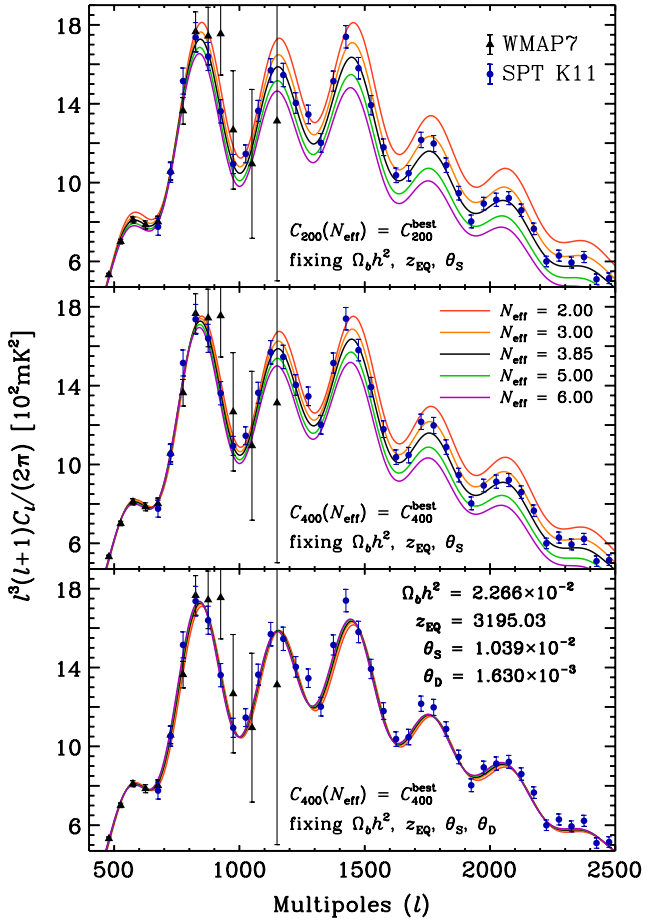

FIG. 1 (color online). *Top panel:* WMAP and SPT power spectrum measurements, and theoretical power spectra normalized at $\ell = 200$. The black (central) curve is for the best-fit ΛCDM + $N_{\rm eff}$ model assuming BBN consistency. The other model curves are for $N_{\rm eff}$ varying from 2 to 6, with ρ_b, θ_s, and $z_{\rm EQ}$ held fixed. Larger $N_{\rm eff}$ corresponds to lower power. *Central panel:* Same as above, except normalized at $\ell = 400$, where the ISW contribution is negligible. We see most of the variation remains. *Bottom panel:* The same as the central panel, except we vary $Y_{\rm P}$ to keep θ_d fixed. The lack of scatter in these spectra compared to those in the middle panel demonstrates that the effect of $N_{\rm eff}$ on small-scale data is largely captured by its impact on the damping scale. We can also begin to see more subtle effects of the neutrinos, most noticeably a phase shift in the acoustic oscillations [23].

phenomenon known as Silk damping. Diffusion causes the drop in power toward high ℓ and makes the power spectrum sensitive to the angular scale of the diffusion length, θ_d. To second order in $\lambda_{\rm mfp}/\lambda$, where $\lambda_{\rm mfp}$ is the photon mean free path, the temperature fluctuations are suppressed by $\exp[-(2r_d/\lambda)^2]$, where the mean squared diffusion distance at recombination is

$$r_d^2 = \pi^2 \int_0^{a_*} \frac{da}{a^3 \sigma_T n_e H} \left[\frac{R^2 + \frac{16}{15}(1+R)}{6(1+R^2)}\right], \qquad (1)$$

where n_e is the number density of free electrons, σ_T is the Thomson cross section, a_* is the scale factor at recombination (defined below), and the factor in square brackets is due to the directional and polarization dependence of Thomson scattering [33,34]. Although Eq. (1) is only an approximation to the diffusion length, it allows an analytic understanding of the dependence of this diffusion length on model parameters [22].

If we approximate a_* as independent of H, then $r_d \propto H^{-0.5}$. This is as expected for a random walk process: the distance increases as the square root of time. Increasing H (which happens when we increase $N_{\rm eff}$) leads to smaller r_d, which would decrease the amount of damping. Why do we see, in Fig. 1, the damping increase as $N_{\rm eff}$ increases?

The answer has to do with how r_s and D_A change to keep θ_s fixed despite the increased expansion rate. The comoving sound horizon is given by

$$r_s = \int_0^{t_*} c_s dt/a = \int_0^{a_*} \frac{c_s da}{a^2 H}. \qquad (2)$$

Since $r_s \propto 1/H$, it responds even more rapidly to changes in H than is the case for r_d. To keep θ_s fixed at the observed value, D_A must also scale as $1/H$. Since D_A decreases by more than would be necessary to keep θ_d fixed, θ_d increases, which means the damping is increased.

To look at it another way, if we knew D_A perfectly, we could use r_s to determine H prior to recombination. But we do not know D_A, largely because we do not know the value of the cosmological constant, or more generally, the density of the dark energy as a function of the scale factor. Instead, we can use the two scales together to form a ratio that is sensitive to H, with no dependence on D_A: $\theta_d/\theta_s = r_d/r_s \propto H^{0.5}$.

Does this explanation hold together quantitatively? To demonstrate that what we are seeing in the power spectrum actually is increased Silk damping (at fixed θ_s), we experiment with also fixing θ_d as $N_{\rm eff}$ increases. The bottom panel of Fig. 1 shows how the angular power spectrum responds to the same variations in $N_{\rm eff}$, only now taken at constant θ_d as well. When we remove the θ_d variation, the impact of the $N_{\rm eff}$ variation almost entirely disappears. We conclude that the variations we are seeing in the top panel are indeed due to the impact of $N_{\rm eff}$ on the amount of Silk damping. A very similar demonstration was provided by Ref. [23].

To keep θ_d fixed as $N_{\rm eff}$ varies, we vary a parameter whose sole impact is on the number density of electrons: the primordial fraction of baryonic mass in helium, $Y_{\rm P}$. Even as early as times when 99% of the photons have yet to last scatter, helium, with its greater binding energy than hydrogen, is almost entirely neutral. Thus, $n_e = X_e(n_p + n_H) = X_e n_b(1 - Y_{\rm P})$, where the first equality defines X_e and we have kept n_b (and thus ρ_b) fixed. The limit of integration in the above equations for r_s and r_d is only slightly affected by changing $Y_{\rm P}$, and thus r_s is largely

unaffected. However, the damping length scales with Y_P, as $r_d \propto (1 - Y_P)^{-0.5}$.

From our analysis, one finds that $r_d/r_s \propto (1 + f_\nu)^{0.25}/\sqrt{1 - Y_P}$, where $f_\nu \equiv \rho_\nu/\rho_\gamma$ is proportional to $N_{\rm eff}$. The first factor arises because increasing H at fixed $z_{\rm EQ}$ means $H^2 \propto (1 + f_\nu)$. Thus, as $N_{\rm eff}$ is varied, we know how to change Y_P to keep r_d/r_s (and hence θ_d/θ_s) fixed.

However, the above analysis requires a small correction for two reasons. First, increased expansion, even if we keep $n_e(a)$ fixed, decreases a_*, because we define a_* following Ref. [35], such that the optical depth to Thomson scattering from here to a_* is unity. Second, recombination is not a process that occurs in chemical equilibrium. As emphasized in Ref. [36], increasing the expansion rate leads to an increase in $n_e(a)$. By numerically studying these effects, which partially cancel each other, we find that $r_d/r_s \propto (1 + f_\nu)^m/\sqrt{1 - Y_P}$ with $m = 0.28$ rather than 0.25.

Note that when varying $N_{\rm eff}$ in Fig. 1, we also vary Y_P as is expected for standard assumptions about BBN, as will be explained below. Following BBN consistency (as opposed to keeping Y_P fixed) increases the damping effect by about 30%.

We should mention that neutrino perturbations do alter the amplitude of the power spectrum at $l \gtrsim 200$ by a (nearly) constant factor [23,37]. The breaking of the $N_{\rm eff}$, ρ_m degeneracy in WMAP data at low $N_{\rm eff}$ is due to the impact of neutrino perturbations, and this is the effect that allowed for an indirect detection of these perturbations as reported in Refs. [38,39].

However, with the inclusion of small-scale data, the perturbations have lost their significance. In Fig. 2, we demonstrate that the $N_{\rm eff}$ constraint from WMAP + SPT is well approximated by combining the WMAP7 data with the information on θ_d/θ_s from WMAP + SPT.

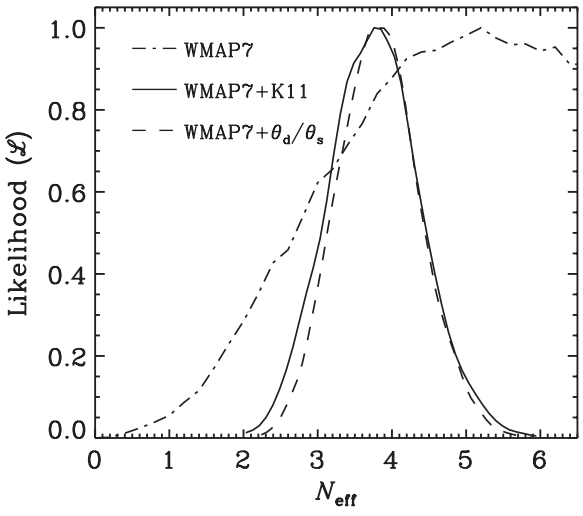

FIG. 2. Probability distribution of $N_{\rm eff}$ using just WMAP data, WMAP + SPT, and WMAP + constraints on θ_d/θ_s from WMAP + SPT (see Table I).

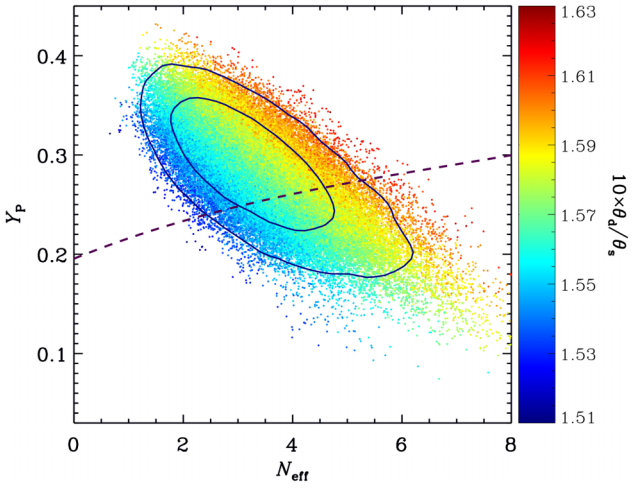

FIG. 3 (color online). The joint likelihood of $N_{\rm eff}$ and Y_P with 68% and 95% confidence contours. Each scattered point in the figure shows one element of the Markov chain with color coding the corresponding value of θ_d/θ_s. The purple dashed line is the BBN consistency line.

Figure 3 provides another way of seeing the importance of θ_d/θ_s to the $N_{\rm eff}$ constraint. From the color coding, one can see that lines of constant θ_d/θ_s run along the major axis of the probability contours. Further, one can see that the BBN consistency line cuts nearly perpendicularly across these lines. This feature explains why the errors on $N_{\rm eff}$ are about 30% smaller if one assumes BBN consistency rather than fixed Y_P. If we abandon BBN consistency and allow Y_P to vary freely, then $N_{\rm eff}$ is allowed to vary along the major axis of the probability contours, and the constraint on $N_{\rm eff}$ loosens considerably, as described in more detail below.

C. Constraining $N_{\rm eff}$ with Y_P free

We do not have a complete analytic understanding of the closing of the contours on the major axis (as opposed to the minor axis) in Fig. 3. We can turn, though, to the lowest panel of Fig. 1 to see that at fixed θ_d/θ_s there is indeed some remaining variation to the power spectra as $N_{\rm eff}$ varies. At least some of this variation is due to the difference in acoustic oscillation phase shift that one gets for neutrinos, relative to the same energy density in photons, due to their free streaming [23].

Another effect important for breaking the degeneracy between Y_P and $N_{\rm eff}$ is due to a high baryon fraction. In our above analysis, we assumed that $z_{\rm EQ}$ is a fixed constant. However, this assumption will break down when $N_{\rm eff}$ decreases to lower values, as it can do if Y_P is allowed to vary freely, while the baryon density remains unchanged. As $N_{\rm eff}$ decreases, to keep $z_{\rm EQ}$ fixed, ω_m would decrease, thus driving up the baryon fraction, ω_b/ω_m. Effects due to the high baryon fraction make it impossible at sufficiently low $N_{\rm eff}$ to find values of $z_{\rm EQ}$, ω_b and ω_b/ω_m that

reproduce the measured power spectra. In an attempt to best accommodate the data, the region of high likelihood departs from constant $z_{\rm EQ}$, as can be seen in the upper panel of Fig. 4, which shows probability contours in the $(1+f_\nu)-\Omega_b/\Omega_m$ plane. The lines are lines of constant $z_{\rm EQ}$ and ω_b. As extra freedom is allowed in the model, allowing $N_{\rm eff}$ to extend to lower values, we can see the expected departure of the probability ridge from the line of constant $z_{\rm EQ}$ and ω_b, mainly due to variation of $z_{\rm EQ}$.

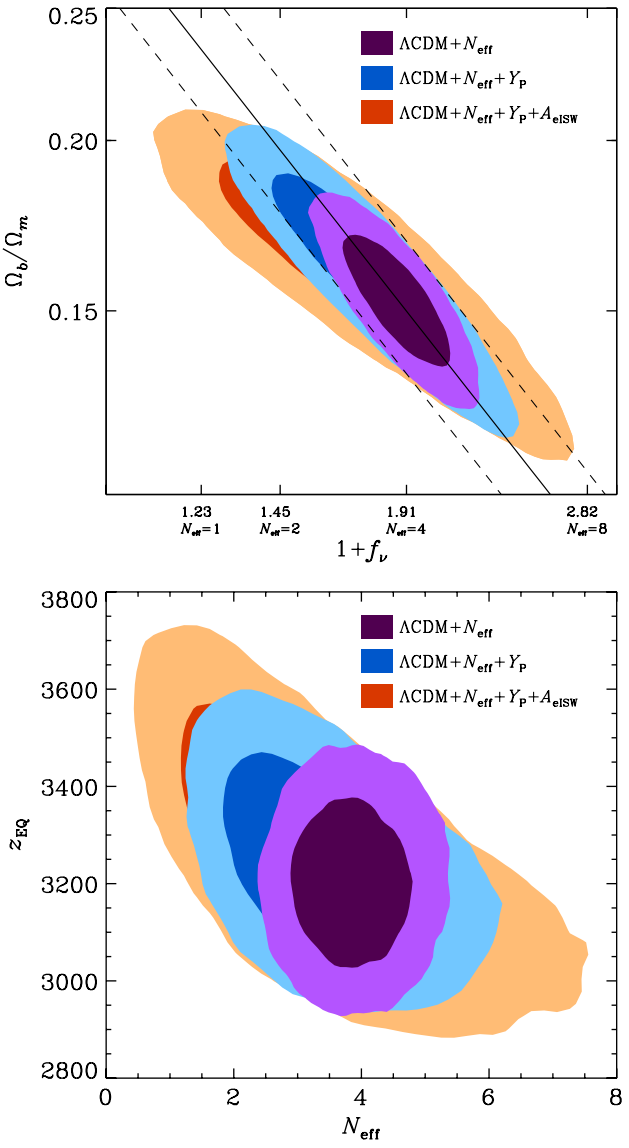

FIG. 4 (color online). Probability contours (68% and 95%) for the cases of BBN consistency (purple), free $Y_{\rm P}$ (blue), and free $Y_{\rm P}$ and $A_{\rm eISW}$ (red). The order (from top to bottom) of the legend of the figure follows the layer order of the contours. *Upper panel:* Baryon fraction, Ω_b/Ω_m vs $(1+f_\nu)$. The solid line is for $100\Omega_b h^2 = 2.267$ and $z_{\rm EQ} = 3200$. Vayring $z_{\rm EQ}$ to 2843 (3557), we get the right (left) dashed line. One can see that the constant $z_{\rm EQ}$ assumption breaks down at high baryon fractions. *Lower panel:* The $N_{\rm eff}$-$z_{\rm EQ}$ plane. Here we can see more directly how the extra freedom degrades the inference of $z_{\rm EQ}$.

A high baryon fraction alters the acoustic dynamics for modes entering the horizon during matter domination, because a large fraction of the matter sourcing the gravitational potentials is feeling pressure support. This pressure support causes potentials to decay, boosting the amplitude of the fluctuations, as happens with the "radiation driving" in the radiation-dominated era. At fixed ω_b, increasing ω_b/ω_m boosts the height of the first peak relative to the second. The existence of this radiation-driving-like effect in the matter-dominated era impacts the ability to constrain $z_{\rm EQ}$. One can see in the lower panel of Fig. 4 how the uncertainty in $z_{\rm EQ}$ increases when $N_{\rm eff}$ is allowed to take on smaller values (as happens when allowing $Y_{\rm P}$ to vary freely). The effect is even greater when allowing further freedom in the model by allowing $A_{\rm eISW}$ to vary, a parameter we will introduce below.

III. CONSTRAINTS ON $N_{\rm eff}$

Here we present constraints on $N_{\rm eff}$ from current data. We begin with our baseline estimates, which are from CMB data alone, assuming the six-parameter ΛCDM model extended by one to allow free $N_{\rm eff}$, with $Y_{\rm P}$ determined by a BBN consistency relation to be discussed below.

We also consider departures from our baseline assumptions. We let $Y_{\rm P}$ vary away from the standard BBN relationship, let $dn_s/d\ln k$ vary away from what is expected from inflation, and allow the early ISW effect to be greater or smaller than expected by introducing a phenomenological scaling parameter, $A_{\rm eISW}$.

Finally, we consider the influence of low-redshift distance measurements on inferences of $N_{\rm eff}$.

A. Baseline constraints

We show our baseline constraints on $N_{\rm eff}$ in the first row of estimates of Table I, which is essentially the same as what the authors of Ref. [4] have found for the same model.

B. Sensitivity to BBN assumptions

The standard assumption is that the baryon-to-photon ratio and $N_{\rm eff}$ are unchanged from BBN through decoupling. However, many processes can change this situation, such as energy injection into the plasma after BBN, which would reduce both ω_b and $N_{\rm eff}$, or a decay of a massive dark species into a relativistic dark species after BBN, which would increase $N_{\rm eff}$ while leaving ω_b unchanged. Here we relax the standard assumption and distinguish the variables with the superscripts DEC (for decoupling) and BBN.

First, we consider the extreme of making no assumptions about BBN and using no light-element abundance data to constrain the BBN quantities. In practice, this simply means allowing $Y_{\rm P}$ to be free. As one would expect from our earlier discussion, allowing $Y_{\rm P}$ to be a free

TABLE I. Sensitivity of inferences of $N_{\rm eff}$ and ω_b to BBN assumptions.

Assumptions	Data	$100\ \omega_b^{\rm BBN}$	$100\ \omega_b^{\rm DEC}$	$100\ \Delta\omega_b$	$N_{\rm eff}^{\rm BBN}$	$N_{\rm eff}^{\rm DEC}$	$\Delta N_{\rm eff}$	ω_m	$10\ \theta_d/\theta_s$
Baseline	CMB	⋯	2.27 ± 0.05	⋯	⋯	3.86 ± 0.62	⋯	0.148 ± 0.012	1.569 ± 0.015
BBN ≠ DEC	CMB	⋯	2.26 ± 0.05	⋯	⋯	$3.28^{+1.09}_{-0.89}$	⋯	$0.140^{+0.018}_{-0.015}$	1.569 ± 0.015
BBN ≠ DEC	CMB + D/H + $Y_{\rm P}^A$	2.29 ± 0.11	2.26 ± 0.06	$-0.023^{+0.123}_{-0.127}$	3.80 ± 0.26	$3.76^{+0.77}_{-0.73}$	$-0.033^{+0.829}_{-0.793}$	0.147 ± 0.014	1.567 ± 0.015
BBN ≠ DEC	CMB + D/H + $Y_{\rm P}^P$	$2.16^{+0.11}_{-0.10}$	2.27 ± 0.05	$0.105^{+0.118}_{-0.124}$	3.09 ± 0.21	$3.93^{+0.79}_{-0.75}$	$0.843^{+0.829}_{-0.794}$	$0.149^{+0.015}_{-0.014}$	1.566 ± 0.015
$\omega_b^{\rm BBN} = \omega_b^{\rm DEC}$	CMB + D/H^{PC}	⋯	2.27 ± 0.05	⋯	3.31 ± 0.58	3.93 ± 0.74	$0.617^{+0.896}_{-0.841}$	0.149 ± 0.014	1.567 ± 0.015

The PC superscript indicates the Pettini and Cooke (2012) inference, A indicates Aver *et al.* (2011), and P indicates Peimbert *et al.* (2007). The dierence $\Delta\omega_b \equiv \omega_b^{\rm DEC} - \omega_b^{\rm BBN}$, and $\Delta N_{\rm eff} \equiv N_{\rm eff}^{\rm DEC} - N_{\rm eff}^{\rm BBN}$.

parameter greatly relaxes the constraints on $N_{\rm eff}^{\rm DEC}$ because of its impact on θ_d/θ_s. This is shown in the second row of Table I.

If we assume standard BBN, we can use measurements of the abundance of deuterium relative to hydrogen, D/H, and $Y_{\rm P}$ to determine $\omega_b^{\rm BBN}$ and $N_{\rm eff}^{\rm BBN}$. Reference [40] provides fitting formulas for the dependence of $Y_{\rm P}$ and D/H on these quantities. Here we present revised ones [41] that incorporate updates in nuclear reaction rate estimates and a neutron lifetime estimate. They are

$$Y_{\rm P} = 0.2381 \pm 0.0006 + [\eta_{10} + 100(S-1)]/625 \quad (3)$$

and

$$10^5 D/H = 2.60(1 \pm 0.06)\left[\frac{6}{\eta_{10} - 6(S-1)}\right]^{1.6}, \quad (4)$$

where

$$\eta_{10} \equiv 10^{10} n_b/n_\gamma = 273.9\omega_b + 100(S-1) \quad \text{and}$$
$$S = [1 + 7(N_{\rm eff} - 3.046)/43]^{1/2}. \quad (5)$$

To calculate $Y_{\rm P}$ as a function of ω_b and $N_{\rm eff}$, we use the default CosmoMC option, which is an interpolation over tables produced using PArthENoPE v1.00 described in Ref. [42], only using Eq. (3) for values outside the bounds of the tables for robustness but very rarely reached. To calculate D/H, we use Eq. (4).

For the measurements of light-element abundances, we mostly follow Ref. [43]. The authors of that source assumed, from a compilation of D/H measurements (see Refs. [44,45] and references therein),

$$\log(D/H) = -4.556 \pm 0.034. \quad (6)$$

We also consider a very recent, and significantly more preicse, D/H measurement by Ref. [46] of

$$\log(D/H) = -4.596 \pm 0.009. \quad (7)$$

Note that significant uncertainty arises from nuclear reaction rate uncertainty. When using D/H measurements, we include the 6% error in Eq. (4) and add it in quadrature with the measurement error.

For helium, Ref. [43] considered two different inferences,

$$Y_P = 0.2573 \pm 0.0033\ (\text{Aver})$$
$$Y_{\rm P} = 0.2477 \pm 0.0029\ (\text{Peimbert}), \quad (8)$$

from Refs. [16,47], respectively; we will do the same.

Including the light-element abundance measurements to help constrain $Y_{\rm P}$ reduces the uncertainty in $N_{\rm eff}^{\rm DEC}$, though it remains comparatively large. Interestingly, the lower $Y_{\rm P}$ measurement, which is the only one of the two consistent with $N_{\rm eff}^{\rm BBN} = 3$, leads to a slightly higher $N_{\rm eff}^{\rm DEC}$ inference. This is because lower $Y_{\rm P}$ values need higher $N_{\rm eff}$ to get the same θ_d/θ_s.

Reference [46] took an inference of the baryon density from Ref. [4] calculated assuming $N_{\rm eff} = 3.046$, combined it with their D/H measurement and the above D/H fitting formula, and found $N_{\rm eff}^{\rm BBN} = 3.0 \pm 0.5$. Thus, they show that their data are consistent with the combination of CMB data and the assumption of $N_{\rm eff}^{\rm BBN} = N_{\rm eff}^{\rm DEC} = 3.046$.

We performed a similar, but different, exercise in which we set $\omega_b^{\rm DEC} = \omega_b^{\rm BBN}$ and estimated both $N_{\rm eff}$ values simultaneously from the CMB and D/H data. There is a small correlation between ω_b and $N_{\rm eff}$ as inferred from the CMB data, which leads to increased ω_b inference when $N_{\rm eff}$ is allowed to vary. The net result is that our exercise leads to a higher value, $N_{\rm eff}^{\rm BBN} = 3.3 \pm 0.6$, with $N_{\rm eff}^{\rm DEC} = 3.93 \pm 0.74$.

We note that our analysis, in which we allow the BBN quantities to be different from the DEC quantities, is for a very general scenario and is therefore missing features that may be important for specific scenarios. For example, in Ref. [48], a scenario was considered in which $N_{\rm eff}$ increases after BBN due to the decay of a fraction of the dark matter into dark radiation. With such a specific choice, one can include in the calculation the details of how this conversion happens over time, and the differences in the dark radiation perturbations from the case of thermally produced neutrinos.

C. Sensitivity to primordial power spectrum assumptions

Another straightforward way to reduce small-scale power is to alter the primordial power spectrum. For the usual power-law assumption, the exponent n_s is sufficiently well determined by low-ℓ data that it cannot mimic

TABLE II. Sensitivity of inferences of $N_{\rm eff}$ to low-redshift distance measurements, $dn_s/d\ln k$, and the phenomenological amplitude of the early ISW effect.

Assumptions	Data	$100\ \omega_b^{\rm DEC}$	$N_{\rm eff}^{\rm DEC}$	$dn_s/d\ln k$	$A_{\rm eISW}$	Ω_Λ	ω_m	$10\ \theta_d/\theta_s$
Baseline	CMB	2.27 ± 0.05	3.86 ± 0.62	...	...	0.737 ± 0.025	0.148 ± 0.012	1.569 ± 0.015
	CMB + BAO	2.25 ± 0.05	3.83 ± 0.60	...	...	0.707 ± 0.012	0.154 ± 0.012	1.569 ± 0.015
	CMB + H_0	2.26 ± 0.04	3.73 ± 0.44	...	...	0.733 ± 0.021	0.147 ± 0.011	1.566 ± 0.012
	CMB + BAO + H_0	2.26 ± 0.04	3.97 ± 0.41	...	...	0.708 ± 0.011	$0.156^{+0.009}_{-0.008}$	1.572 ± 0.011
$dn_s/d\ln k$ free	CMB	2.21 ± 0.07	$2.97^{+0.91}_{-0.80}$	-0.025 ± 0.020	...	0.704 ± 0.041	$0.138^{+0.014}_{-0.012}$	$1.547^{+0.022}_{-0.021}$
$dn_s/d\ln k$ free	CMB + BAO + H_0	2.25 ± 0.04	3.76 ± 0.43	-0.015 ± 0.013	...	0.706 ± 0.011	0.153 ± 0.009	1.566 ± 0.012
$A_{\rm eISW}$ free	CMB	2.29 ± 0.08	3.92 ± 0.65	...	0.979 ± 0.055	0.741 ± 0.028	0.149 ± 0.012	1.568 ± 0.015
$A_{\rm eISW}$ free	CMB + H_0	2.26 ± 0.06	3.72 ± 0.44	...	0.990 ± 0.048	0.734 ± 0.022	0.147 ± 0.011	1.565 ± 0.013
$Y_{\rm P}$, $A_{\rm eISW}$ free	CMB	2.24 ± 0.11	$3.07^{+1.59}_{-1.20}$	...	1.011 ± 0.076	$0.726^{+0.035}_{-0.041}$	$0.137^{+0.024}_{-0.018}$	1.569 ± 0.015

the damping effect of $N_{\rm eff}$. However, if we allow for n_s to have a logarithmic scale dependence so that $n_s(k) = n_s(k_*) + \ln(k/k_*)dn_s/d\ln k$ for some constant $dn_s/d\ln k$, then the resulting power spectra can better mimic the effects of $N_{\rm eff}$. As a result, if we marginalize over $dn_s/d\ln k$, we increase the uncertainty in $N_{\rm eff}$, as can be seen in Table II.

D. Importance of the early ISW effect

The anisotropy field today can be written as an integration over perturbation variables on the past light cone. Doing so can be useful both computationally [49] and for analytic understanding. Writing the Fourier- and Legendre-transformed radiation transfer function as such an integral (ignoring the polarization dependence of Thomson scattering for simplicity), one gets

$$\begin{aligned}\Theta_l(k) = &\int_0^{\eta_0} d\eta g(\eta)[\Theta_0(k,\eta) + \Psi(k,\eta)]j_l[k(\eta_0-\eta)] \\ &- \int_0^{\eta_0} d\eta g(\eta)\frac{iv_b(k,\eta)}{k}\frac{d}{d\eta}j_l[k(\eta_0-\eta)] \\ &+ \int_0^{\eta_0} d\eta f(z(\eta), A_{\rm eISW}) \\ &\times e^{-\tau}[\dot\Psi(k,\eta) - \dot\Phi(k,\eta)]j_l[k(\eta_0-\eta)]. \qquad (9)\end{aligned}$$

See Ref. [50] for definitions. The final integral is the so-called integrated Sachs-Wolfe (ISW) effect. The other terms are only important when the visibility function $g(\eta)$ is nonzero, whereas the ISW term gets contributions along the whole line of sight between here and recombination, where τ starts to get very large. The gravitational potential time derivatives are zero for a universe dominated by cold dark matter. They are significantly nonzero at early times, as the radiation density is still a significant contributor to the expansion rate (the early ISW effect), and then again at late times when dark energy becomes important (the late ISW effect).

In Eq. (9), we have introduced the parameter $A_{\rm eISW}$ so we can artificially vary the amplitude of the early ISW effect. The function $f(z(\eta), A_{\rm eISW}) = A_{\rm eISW}$ when the redshift, $z > 30$, and otherwise equals 1. This use of $A_{\rm eISW}$ is very similar to the use of $A_{\rm lens}$ to artificially change the amplitude of the lensing potential power spectrum altering the CMB power spectrum. We might have chosen f to go as the square root of $A_{\rm eISW}$ so that $A_{\rm eISW}$ is scaling the ISW power (just as $A_{\rm lens}$ scales up the lensing power). However, a significant impact of the ISW term in Eq. (9) comes from its correlation with the other terms in the equation. Thus, there is no way to render the total contribution of early ISW to the power scale as a single power of $A_{\rm eISW}$.

The greater the amount of radiation relative to matter at recombination, the greater the amplitude of the early ISW effect. Thus, increasing $N_{\rm eff}$ (with ω_m held fixed) would increase the amplitude of the early ISW effect. This relationship between $N_{\rm eff}$ and the early ISW effect led Ref. [32] to cite the ISW effect as the reason the CMB is sensitive to $N_{\rm eff}$.

To quantitatively investigate the impact of the ISW effect, we could perform the exercise of turning it off artificially. But turning off the ISW effect would so radically change the first peak (dropping it in power by 28%) that we instead chose to investigate by letting $A_{\rm eISW}$ be a free parameter. If the ISW effect is playing an important role in constraining $N_{\rm eff}$, then if we let it be a free parameter, those constraints will degrade and we will also see a strong correlation between the two parameters.

We show probability contours in the $N_{\rm eff}$-$A_{\rm eISW}$ plane in Fig. 5 for the case that $Y_{\rm P}$ follows the BBN consistency relation and the case that $Y_{\rm P}$ is free. For the BBN-consistent case, the constraint on $N_{\rm eff}$ degrades by less than 5% from $N_{\rm eff} = 3.86 \pm 0.62$ to $N_{\rm eff} = 3.92 \pm 0.65$. The degradation on $N_{\rm eff}$ becomes negligible when the H_0 prior is combined with CMB data, as shown in Table II. This is consistent with what we have found in discussions on Fig. 2—that the constraint on $N_{\rm eff}$ is almost entirely due to the measurement of θ_d/θ_s.

However, when $Y_{\rm P}$ is allowed to vary freely, the θ_d/θ_s constraint can no longer determine $N_{\rm eff}$ because of the degeneracy with $Y_{\rm P}$. In this case, the region of the spectrum affected by ISW is more important for determining $N_{\rm eff}$. When $A_{\rm eISW}$ is also allowed to be free, it can modulate the height of the first acoustic peak and hence the baryon fraction, which leads to a wider range of $Y_{\rm P}$ variation due to its degeneracy with ω_b during recombination and a wider $N_{\rm eff}$ constraint with fixed θ_d/θ_s. In Fig. 5, we do

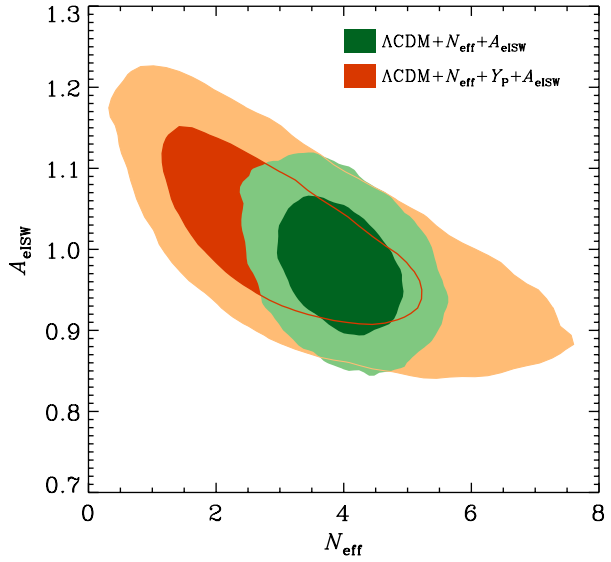

FIG. 5 (color online). Probability contours (68% and 95%) in the $A_{\rm eISW}$-$N_{\rm eff}$ plane, assuming BBN consistency (green, tighter contours) and free $Y_{\rm P}$ (red, broader contours). The order (from top to bottom) of the legend of the figure follows the layer order of the contours. We see in the BBN-consistent case that the constraint on $N_{\rm eff}$ persists despite the freedom in the phenomenological amplitude of the early ISW effect. For the case of free $Y_{\rm P}$, $A_{\rm eISW}$ is important for constraining $N_{\rm eff}$; letting the amplitude vary freely degrades the constraints on $N_{\rm eff}$ somewhat, especially at low $N_{\rm eff}$.

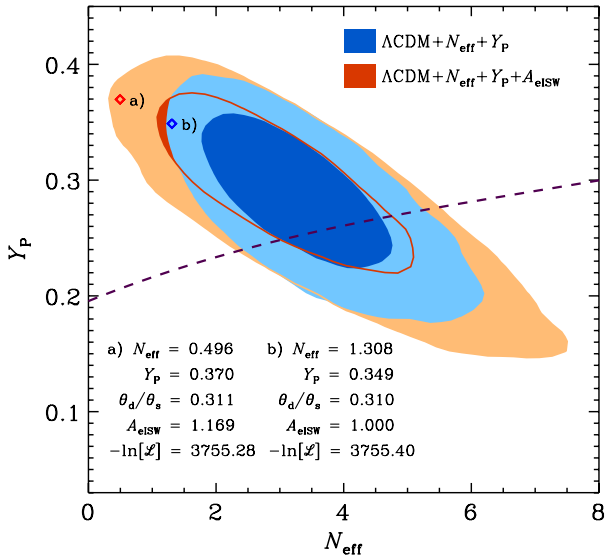

FIG. 6 (color online). Allowing $A_{\rm eISW}$ to vary stretches out the contours in the $Y_{\rm P}$ plane in the direction not constrained by θ_d/θ_s. If we assume BBN consistency, though (the dashed line), then it has very little impact on the constraint on $N_{\rm eff}$. Along the direction of constant θ_d/θ_s, two samples, a) and b), in the two Markov chains are picked up with almost identical likelihood values. The parameters of interest of these two samples are listed, and the corresponding power spectra are plotted in Fig. 7 with the $A_{\rm eISW}$ modulation turned off and on.

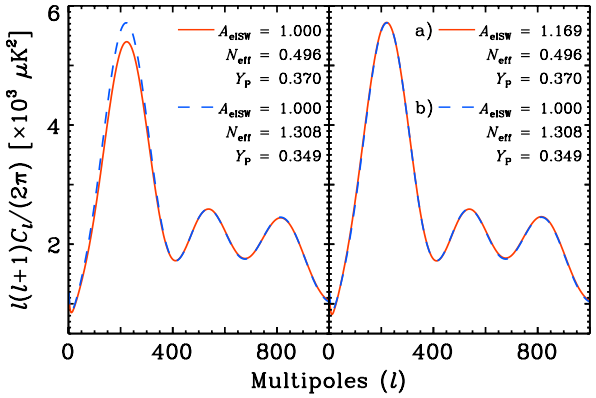

FIG. 7 (color online). The power spectra of the two samples shown in Fig. 6 with the $A_{\rm eISW}$ modulation turned off (on) in the left (right) panel. In this figure, we see explicitly how allowing $A_{\rm eISW}$ to be artificially free weakens the lower bound on $N_{\rm eff}$ in the case that $Y_{\rm P}$ is free.

see a significantly enhanced degeneracy between $A_{\rm eISW}$ and $N_{\rm eff}$ when $Y_{\rm P}$ is allowed to be free. From Fig. 6, we can see that marginalizing over $A_{\rm eISW}$ does indeed loosen up the $N_{\rm eff}$, $Y_{\rm P}$ contour. The constraint on $N_{\rm eff}$ is degraded from $N_{\rm eff} = 3.28^{+1.09}_{-0.89}$ to $N_{\rm eff} = 3.07^{+1.59}_{-1.20}$, as shown in Tables I and II. One can see explicitly in Fig. 7 how letting $A_{\rm eISW}$ vary allows lower $N_{\rm eff}$ and higher $Y_{\rm P}$ than would otherwise be possible.

We also see from Fig. 6 that marginalizing over $A_{\rm eISW}$ does little to expand the minor axis of the contours. As we have emphasized, the constraint along this axis is due to the constraint on θ_d/θ_s. Along the major axis, the early ISW effect does play an important role in breaking the $N_{\rm eff}$-$Y_{\rm P}$ degeneracy. Other effects important in breaking this degeneracy include those coming from neutrino perturbations [23] and high baryon fraction, as discussed in Sec. II C.

IV. IMPLICATIONS FOR LOW-REDSHIFT DISTANCE MEASUREMENTS

We now consider the implications of CMB measurements in the context of variable $N_{\rm eff}$ for low-redshift measurements.

Let us first consider the effect on the expansion rate at low redshift for the ΛCDM + $N_{\rm eff}$ cosmology. Increasing $N_{\rm eff}$, with the resulting increase in $\omega_m \propto (1 + f_\nu)$ (to keep $z_{\rm EQ}$ fixed) increases the expansion rate through the matter-dominated era. Further, in order to adjust D_A to keep θ_s fixed (given the decrease in r_s), the energy density in the cosmological constant, ω_Λ, must increase as well. With the energy density in both components important at low redshift increasing, $H(z)$ increases for all redshifts in the low-redshift (matter-dominated and later) regime.

Note that if we can ignore changes to the limit of integration in Eq. (2), then we expect $r_s(z_*) \propto (1 + f_\nu)^{-0.5}$. With this scaling, we then expect $D_A(z_*) \propto (1 + f_\nu)^{-0.5}$

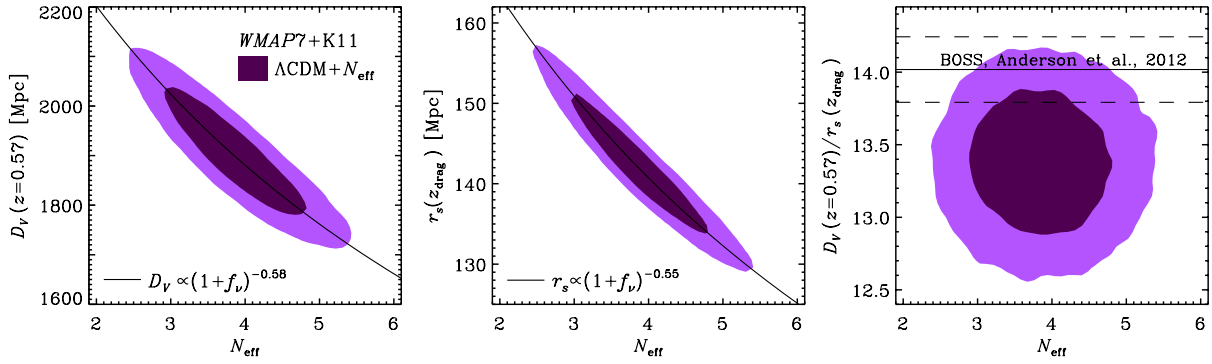

FIG. 8 (color online). *Left panel:* Contours of constant probability indicating the 68% and 95% confidence regions in the $N_{\rm eff} - D_V(z = 0.57)$ plane. The solid line shows the major correlation direction of $D_V(z = 0.57) \propto (1 + f_\nu)^{-0.58}$ with the index best-fitted from the Markov chain. *Middle panel:* Probability contours in the $N_{\rm eff} - r_s(z_{\rm drag})$ plane; the solid line holds the best-fit correlation direction $r_s(z_{\rm drag}) \propto (1 + f_\nu)^{-0.55}$. *Right panel:* The relationship between $N_{\rm eff}$ and the ratio, D_V/r_s. The latest BOSS BAO data point [21] is plotted with the dashed line showing its 1σ error, which is rescaled by multiplying by the r_s rescaling factor 154.66/150.82.

to keep θ_s fixed. The only way to achieve that scaling in the ΛCDM model is to have the dark energy density ω_Λ scale in exactly the same way as ω_m. Hence $H(z)$, and therefore also $D_A(z)$, scales the same way at all redshifts. If $z_{\rm drag}$ also has no variation with $N_{\rm eff}$, then the net result is that the BAO observables $D_A(z)/r_s(z_{\rm drag})$ and $H(z) * r_s(z_{\rm drag})$ have no dependence on $N_{\rm eff}$. Note that $z_{\rm drag}$ is the epoch of photon-baryon decoupling defined as in Ref. [51].

In practice, there are many corrections to the above analysis—e.g., the correlation between $z_{\rm drag}$ and $N_{\rm eff}$—but they are all small, and the net result is very little dependence of the BAO observables on $N_{\rm eff}$. We can see this in Table II, where adding in just BAO data makes very little difference to the $N_{\rm eff}$ inference. Another consequence of ω_Λ scaling similarly to ω_m is that Ω_Λ does not scale with $N_{\rm eff}$.

Figure 8 quantitatively supports the above discussion. We compute the quantity $D_V \equiv (D_A^2 cz/H(z))^{1/3}$ at the redshift $z = 0.57$, where the latest BAO data were effectively measured [21]. We see that $D_V(z = 0.57) \propto (1 + f_\nu)^{-0.58}$, $r_s(z_{\rm drag}) \propto (1 + f_\nu)^{-0.55}$; i.e., they both scale nearly as $(1 + f_\nu)^{-0.5}$. And their scalings are so similar that the ratio of the two quantities shows no noticeable correlation with $N_{\rm eff}$. In the case of WMAP7 + K11 + BAO + H_0, we get $\sigma(N_{\rm eff}) = 0.41$, compared to $\sigma(N_{\rm eff}) = 0.42$ in K11 [4] for our baseline model. The only difference comes from the latest BAO data point, which shows a little tension with the D_V/r_s inference from the CMB data [52].

What *are* sensitive to $N_{\rm eff}$ at low redshift are absolute distance measures that are not calibrated with r_s. The inference of H_0, given ΛCDM (with standard radiation content) calibrated with the WMAP7 and SPT data, is $h = 0.710 \pm 0.021$. This is 1.17σ lower than the Riess *et al.* (2011) value of $h = 0.738 \pm 0.024$ [19]. Increasing $N_{\rm eff}$ to the higher value preferred by the CMB data alone brings these two inferences into better agreement. One can see the impact of the Riess *et al.* measurement on the reduced uncertainty in $N_{\rm eff}$ in the table entries I and II for the ΛCDM + $N_{\rm eff}$ cosmology; including the Riess *et al.* measurement drops the uncertainty by about 50%.

Varying $N_{\rm eff}$ thus changes the ΛCDM, CMB-calibrated predictions for H_0, without much change in the predictions for the BAO data—consistent with the analysis in Ref. [53]. Increasing $N_{\rm eff}$ thus can eliminate the tension between the BAO data and the Riess *et al.* H_0 measurement, as pointed out in Ref. [20].

The case of $dn_s/d\ln k$ free allows us to see this preference of the low-redshift data for the $H(z)$ that comes from an increased $N_{\rm eff}$. With CMB data alone, letting the running vary leads to a downward shift in the central value for $N_{\rm eff}$. Adding in the H_0 and BAO measurements shifts the preferred value for $N_{\rm eff}$ back up towards 4.

Increasing $N_{\rm eff}$ also has implications for the growth of structure. Increasing $N_{\rm eff}$ leads to an increase in ω_m, which in turn decreases ω_b/ω_m. Decreasing the baryon fraction decreases the pressure support felt by matter prior to recombination, thereby boosting the growth of structure on scales smaller than the sound horizon at recombination; i.e., scales smaller than about 150 Mpc [54]. Therefore, increasing $N_{\rm eff}$ increases cluster abundances that are sensitive to the power spectrum amplitude on ~10 Mpc scales. This effect can be seen in joint estimates of m_ν (which has the opposite impact on small-scale power) and $N_{\rm eff}$ from cluster abundances in Ref. [55] and also in Refs. [56,57].

V. CONCLUSION

There are several ways that massless neutrinos impact the anisotropy of the cosmic microwave background. Here we have shown that current CMB constraints on $N_{\rm eff}$ are dominated by the impact of the neutrino energy density on the expansion rate. Although θ_s is sensitive to this change in expansion rate from $N_{\rm eff}$, its simultaneous sensitivity to

the distance to last scattering greatly limits how well $N_{\rm eff}$ can be reconstructed from it alone. Measuring the damping tail region has allowed a measurement of θ_d as well. Since the response of θ_d to the expansion rate is different from the response of θ_s, their ratio (which is independent of the distance to last scattering) is sensitive to the expansion rate.

The above analysis assumes that $Y_{\rm P}$ follows the BBN consistency relation. Since $Y_{\rm P}$ also alters θ_d, allowing it to vary freely introduces a near degeneracy between $N_{\rm eff}$ and $Y_{\rm P}$. This near degeneracy is broken by a number of physical effects at low $N_{\rm eff}$, including the early ISW effect and the effects of a high baryon fraction. At high $N_{\rm eff}$, the acoustic oscillation phase shifts probably play an important role, although we have not quantitatively confirmed this hypothesis.

We defined a phenomenological scaling parameter of the early ISW effect, $A_{\rm eISW}$. We used it to study how much the early ISW effect plays a role in the $N_{\rm eff}$ constraint. After marginalizing over $A_{\rm eISW}$, the constraint on $N_{\rm eff}$ degrades little for the BBN-consistent scenario. However, as just noted above, the early ISW effect does contribute to constraints on $N_{\rm eff}$ when $Y_{\rm P}$ is allowed to vary freely. We found that, assuming BBN consistency, $A_{\rm eISW} = 0.979 \pm 0.055$—a highly significant (though model dependent) detection of the early ISW effect.

We tested the consistency of inferences of ω_b, $N_{\rm eff}$ and $Y_{\rm P}$ from CMB data with inferences from light-element abundance measurements and BBN theory. We see no strong evidence for any inconsistency, though the bounds are quite loose. For the most discrepant case, we find $N_{\rm eff}^{\rm DEC} - N_{\rm eff}^{\rm BBN} = 0.84^{+0.83}_{-0.79}$. We note that a simultaneous inference of $N_{\rm eff}^{\rm BBN}$ and $N_{\rm eff}^{\rm DEC}$ from the CMB and the new Pettini and Cooke D/H measurement results in a $N_{\rm eff}^{\rm BBN}$ more consistent with 4 than is the case for the similar exercise performed in Ref. [46].

We considered the impact of low-redshift distance-redshift relation measurements on the determination of $N_{\rm eff}$. We found that BAO data are not very sensitive to $N_{\rm eff}$ because D_V and r_s scale similarly with $N_{\rm eff}$. The same cancellation does not occur for distance measures that calibrate independently of the CMB, such as the Hubble constant determination in Ref. [19].

We will have tighter measurements from the forthcoming analysis of the entire SPT survey, and we expect improvements to come from Planck in early 2013. We project that the error on $N_{\rm eff}$ will reduce to $\sim$0.33 using simulated full-survey SPT data combined with existing WMAP and H_0 data, and will reduce further to $\sim$0.20 using simulated Planck data and existing H_0 data, assuming the Planck data and foreground model of Ref. [58], consistent with the forecasts of Refs. [23,59] and Ref. [59].

ACKNOWLEDGMENTS

We thank A. Albrecht, B. Benson, O. Doré, E. Komatsu, M. Luty, J. Ruhl, L. Strigari, A. Vikhlinin and M. White for useful conversations. We acknowledge support from NSF Grants No. 0709498 and No. ANT-0638937. We used CosmoMC [60].

[1] C. L. Reichardt, P. A. R. Ade, J. J. Bock, J. R. Bond, J. A. Brevik, C. R. Contaldi, M. D. Daub, J. T. Dempsey, J. H. Goldstein, W. L. Holzapfel *et al.*, Astrophys. J. **694**, 1200 (2009).

[2] S. Das, T. A. Marriage, P. A. R. Ade, P. Aguirre, M. Amiri, J. W. Appel, L. F. Barrientos, E. S. Battistelli, J. R. Bond, B. Brown *et al.*, Astrophys. J. **729**, 62 (2011).

[3] J. Dunkley, R. Hlozek, J. Sievers, V. Acquaviva, P. A. R. Ade, P. Aguirre, M. Amiri, J. W. Appel, L. F. Barrientos, E. S. Battistelli *et al.*, Astrophys. J. **739**, 52 (2011).

[4] R. Keisler, C. L. Reichardt, K. A. Aird, B. A. Benson, L. E. Bleem, J. E. Carlstrom, C. L. Chang, H. M. Cho, T. M. Crawford, A. T. Crites *et al.*, Astrophys. J. **743**, 28 (2011).

[5] P. C. de Holanda and A. Y. Smirnov, Phys. Rev. D **83**, 113011 (2011).

[6] W. Fischler and J. Meyers, Phys. Rev. D **83**, 063520 (2011).

[7] L. M. Krauss, C. Lunardini, and C. Smith, arXiv:1009.4666.

[8] S. Galli, M. Martinelli, A. Melchiorri, L. Pagano, B. D. Sherwin, and D. N. Spergel, Phys. Rev. D **82**, 123504 (2010).

[9] K. Nakayama, F. Takahashi, and T. T. Yanagida, Phys. Lett. B **697**, 275 (2011).

[10] Jungman *et al.* [61] first pointed out that the number of species of relativistic neutrinos could be measured from the CMB.

[11] The effective number of neutrinos is defined so that the neutrino and photon energy densities are related by $\rho_\nu = N_{\rm eff} 7/8 (4/11)^{4/3} \rho_\gamma$.

[12] S. Hannestad, A. Mirizzi, G. G. Raffelt, and Y. Y. Y. Wong, J. Cosmol. Astropart. Phys. 08 (2010) 001.

[13] W. Fischler and W. T. Garcia, J. High Energy Phys. 06 (2011) 046.

[14] Y. I. Izotov and T. X. Thuan, Astrophys. J. Lett. **710**, L67 (2010).

[15] E. Aver, K. A. Olive, and E. D. Skillman, J. Cosmol. Astropart. Phys. 05 (2010) 003.

[16] E. Aver, K. A. Olive, and E. D. Skillman, J. Cosmol. Astropart. Phys. 03 (2011) 043.

[17] A. A. Aguilar-Arevalo, C. E. Anderson, S. J. Brice, B. C. Brown, L. Bugel, J. M. Conrad, R. Dharmapalan, Z. Djurcic, B. T. Fleming, R. Ford *et al.*, Phys. Rev. Lett. **105**, 181801 (2010).

[18] G. Mention, M. Fechner, T. Lasserre, T. A. Mueller, D. Lhuillier, M. Cribier, and A. Letourneau, Phys. Rev. D **83**, 073006 (2011).

[19] A. G. Riess, L. Macri, S. Casertano, H. Lampeitl, H. C. Ferguson, A. V. Filippenko, S. W. Jha, W. Li, and R. Chornock, Astrophys. J. **730**, 119 (2011).

[20] K. T. Mehta, A. J. Cuesta, X. Xu, D. J. Eisenstein, and N. Padmanabhan, arXiv:1202.0092.

[21] L. Anderson, E. Aubourg, S. Bailey, D. Bizyaev, M. Blanton, A. S. Bolton, J. Brinkmann, J. R. Brownstein, A. Burden, A. J. Cuesta *et al.*, Mon. Not. R. Astron. Soc. **428**, 1036 (2013).

[22] W. Hu and M. White, Astrophys. J. **471**, 30 (1996).

[23] S. Bashinsky and U. Seljak, Phys. Rev. D **69**, 083002 (2004).

[24] An exception is the breaking of the $Y_{\rm P}$-$N_{\rm eff}$ degeneracy, to be discussed later.

[25] Energy densities today are often expressed as, e.g., $\Omega_b h^2 = \rho_b/(1.879 \times 10^{-29}\ {\rm g/cm^3})$.

[26] W. Hu and S. Dodelson, Annu. Rev. Astron. Astrophys. **40**, 171 (2002).

[27] W. Hu, M. Fukugita, M. Zaldarriaga, and M. Tegmark, Astrophys. J. **549**, 669 (2001).

[28] J. C. Mather, E. S. Cheng, R. E. Eplee, Jr., R. B. Isaacman, S. S. Meyer, R. A. Shafer, R. Weiss, E. L. Wright, C. L. Bennett, N. W. Boggess *et al.*, Astrophys. J. Lett. **354**, L37 (1990).

[29] $\Omega_m \equiv 8\pi G\rho_m/(3H_0^2)$.

[30] E. Komatsu, J. Dunkley, M. R. Nolta, C. L. Bennett, B. Gold, G. Hinshaw, N. Jarosik, D. Larson, M. Limon, L. Page *et al.*, Astrophys. J. Suppl. Ser. **180**, 330 (2009).

[31] $c_s^2 = \partial P/\partial\rho = 1/[3(1+R)]$, with $R = 3\rho_b(z)/(4\rho_\gamma(z))$.

[32] R. Bowen, S. H. Hansen, A. Melchiorri, J. Silk, and R. Trotta, Mon. Not. R. Astron. Soc. **334**, 760 (2002).

[33] N. Kaiser, Mon. Not. R. Astron. Soc. **202**, 1169 (1983).

[34] M. Zaldarriaga and D. D. Harari, Phys. Rev. D **52**, 3276 (1995).

[35] W. Hu and N. Sugiyama, Astrophys. J. **444**, 489 (1995).

[36] O. Zahn and M. Zaldarriaga, Phys. Rev. D **67**, 063002 (2003).

[37] W. Hu, D. Scott, N. Sugiyama, and M. White, Phys. Rev. D **52**, 5498 (1995).

[38] R. Trotta and A. Melchiorri, Phys. Rev. Lett. **95**, 011305 (2005).

[39] F. De Bernardis, L. Pagano, P. Serra, A. Melchiorri, and A. Cooray, J. Cosmol. Astropart. Phys. 06 (2008) 013.

[40] V. Simha and G. Steigman, J. Cosmol. Astropart. Phys. 06 (2008) 016.

[41] G. Steigman (private communication).

[42] O. Pisanti, A. Cirillo, S. Esposito, F. Iocco, G. Mangano, G. Miele, and P. D. Serpico, Comput. Phys. Commun. **178**, 956 (2008).

[43] K. M. Nollett and G. P. Holder, arXiv:1112.2683.

[44] M. Pettini, B. J. Zych, M. T. Murphy, A. Lewis, and C. C. Steidel, Mon. Not. R. Astron. Soc. **391**, 1499 (2008).

[45] M. Fumagalli, J. M. O'Meara, and J. X. Prochaska, Science **334**, 1245 (2011).

[46] M. Pettini and R. Cooke, arXiv:1205.3785.

[47] M. Peimbert, V. Luridiana, and A. Peimbert, Astrophys. J. **666**, 636 (2007).

[48] O. E. Bjaelde, S. Das, and A. Moss, J. Cosmol. Astropart. Phys. 10 (2012) 017.

[49] U. Seljak and M. Zaldarriaga, Astrophys. J. **469**, 437 (1996).

[50] S. Dodelson, *Modern Cosmology* (Academic Press, Elsevier Science, New York, 2003).

[51] A. Meiksin, M. White, and J. A. Peacock, Mon. Not. R. Astron. Soc. **304**, 851 (1999).

[52] Note that Anderson *et al.* [21] report D_V/r_s for an r_s given by the fitting formula of Ref. [54]. We have adjusted the reported value for comparison to D_V/r_s calculated with our definition of r_s by multiplying it by 154.66/150.82. See Ref. [20].

[53] D. Eisenstein and M. White, Phys. Rev. D **70**, 103523 (2004).

[54] D. J. Eisenstein and W. Hu, Astrophys. J. **496**, 605 (1998).

[55] B. A. Benson, T. de Haan, J. P. Dudley, C. L. Reichardt, K. A. Aird, K. Andersson, R. Armstrong, M. Bautz, M. Bayliss, G. Bazin *et al.*, Astrophys. J. **763**, 147 (2013).

[56] J. Hamann, S. Hannestad, G. G. Raffelt, I. Tamborra, and Y. Y. Y. Wong, Phys. Rev. Lett. **105**, 181301 (2010).

[57] J. Hamann, S. Hannestad, G. G. Raffelt, and Y. Y. Y. Wong, J. Cosmol. Astropart. Phys. 09 (2011) 034.

[58] M. Millea, O. Doré, J. Dudley, G. Holder, L. Knox, L. Shaw, Y. Song, and O. Zahn, Astrophys. J. **746**, 4 (2012).

[59] S. Hannestad, H. Tu, and Y. Y. Wong, J. Cosmol. Astropart. Phys. 06 (2006) 025.

[60] A. Lewis and S. Bridle, Phys. Rev. D **66**, 103511 (2002).

[61] G. Jungman, M. Kamionkowski, A. Kosowsky, and D. N. Spergel, Phys. Rev. Lett. **76**, 1007 (1996).